Engineered Science

RESEARCH PAPER

View Article Online

Improved Thermal Stabilities, Ablation and Mechanical Properties for Carbon Fibers/Phenolic Resins Laminated Composites Modified by Silicon-containing Polyborazine

Hui Zhao,[1,2] Lixin Chen,*[1,2] Jin Yun,[1,2] Lin Tang,[1,2] Ziyou Wen,[1,2] Xiao Zhang[1,2] and Junwei Gu*[1,2,3]

Synthesized ceramic precursor of silicon-containing polyborazine (SPBZ) was introduced to fabricate the modified phenolic resins (SPBZ-PR), which was then performed as resin matrix to obtain carbon fibers reinforced SPBZ-PR (CF/SPBZ-PR) laminated composites *via* hot-compression. The incorporation of SPBZ could improve the thermal stabilities of PR, and the optimal decomposition temperature at 5% weight loss (T_5) of the $SPBZ_{15}$-PR (15 wt% of phenol to SPBZ) was increased to 406.8°C and the char yield at 1200°C still retained 70.3%, owing to borazine ring and formed SiO_x structure during pyrolysis process. Furthermore, the CF/$SPBZ_{15}$-PR laminated composites presented relatively higher ILSS, more excellent ablation properties and shape retention abilities than that of CF/PR laminated composites. The corresponding linear and mass ablation rate were both decreased from 0.013 mm/s and 0.033 g/s for CF/PR laminated composites to 0.0079 mm/s and 0.025 g/s, decreased by 39.2% and 24.2%, respectively.

Keywords: Phenolic resins; Ceramic precursor; Carbon fibers; Thermal stabilities; Ablation resistance

Received 17th May 2018, Accepted 27th May 2018

DOI: 10.30919/es8d726

1. Introduction

Phenolic resins (PR) can be applied as insulation materials, fire resistance materials and ablative materials, owing to their low smoke rate & high char yield during combustion, low cost and good processability.[1–5] Especially, compared to that of other thermosetting resins (epoxy,[6–8] polyimide,[9,10] cyanate ester[11] and bismaleimide[12]), *etc*., PR can be usually used as ablation resistant resin matrix for advanced polymeric composites in the fields of aerospace industries and modern high-tech weaponry, *etc*..[13] However, with the rapid development of space, aviation and military industries, it is difficult for common PR matrix to meet the higher requirements.[14,15]

Extensive efforts have been performed to improve the heat resistances of PR matrix. And the adopted methods can be divided into physical blending and chemical copolymerization. At present, BC_4,[16] BN,[17–19] SiO_2,[20,21] carbon nanotubes[22–24] and graphene,[25–28] have been used to modify PR through physical blending method. Although the thermal stabilities of the modified PR could be improved, the corresponding mechanical properties were unsatisfactory due to phase separation. Fortunately, chemical copolymerization presents promising method to solve the above phase separation, which can also enhance the thermal stabilities of the PR matrix but hardly decrease the mechanical properties. Generally, copolymerization modification mainly includes element and structural modification. Element modification is introducing certain heteroatom (boron, silicon, phosphorus or molybdenum, *etc*.,)[29–32] into PR matrix. Herein, boron modified PR possesses the optimal comprehensive properties.[33,34] In our previous work, the corresponding char yield of boron modified PR at 800°C could reach to 67.9%.[35] Structural modification is introducing excellent thermostable structure (such as aromatic or maleimide structure) into PR matrix. Ceramic precursor possesses excellent structural stability and high ceramic yield (> 800°C),[36] which can efficiently improve the char yield of PR matrix.[37] Investigations revealed that six-membered borazine ring could steadily exist under higher temperatures.[38]

In our present work, ceramic precursor of silicon-containing polyborazine (SPBZ) was firstly synthesized from borontrichloride and hexamethyldisilazane. Furthermore, the SPBZ was introduced into PR matrix to fabricate the modified phenolic resin (SPBZ-PR) *via* condensation polymerization. Finally, carbon fibers (CF) were then introduced into SPBZ-PR matrix to obtain the corresponding CF/SPBZ-PR laminated composites by the method of hot-compression. Nuclear magnetic resonance (NMR), thermal gravimetric analyses

[1] *Research & Development Institute of Northwestern Polytechnical University in Shenzhen, Guangdong, 518057, P.R. China. E-mail: lixin@nwpu.edu.cn, gjw@nwpu.edu.cn, nwpugjw@163.com*

[2] *MOE Key Laboratory of Material Physics and Chemistry under Extraordinary Conditions, Shaanxi Key Laboratory of Macromolecular Science and Technology, Department of Applied Chemistry, School of Science, Northwestern Polytechnical University, Xi' an, Shaanxi, 710072, P.R. China*

[3] *Institute of Intelligence Material and Structure, Institute of Unmanned Systems, Northwestern Polytechnical University, Xi' an, Shaanxi, 710072, P.R. China*

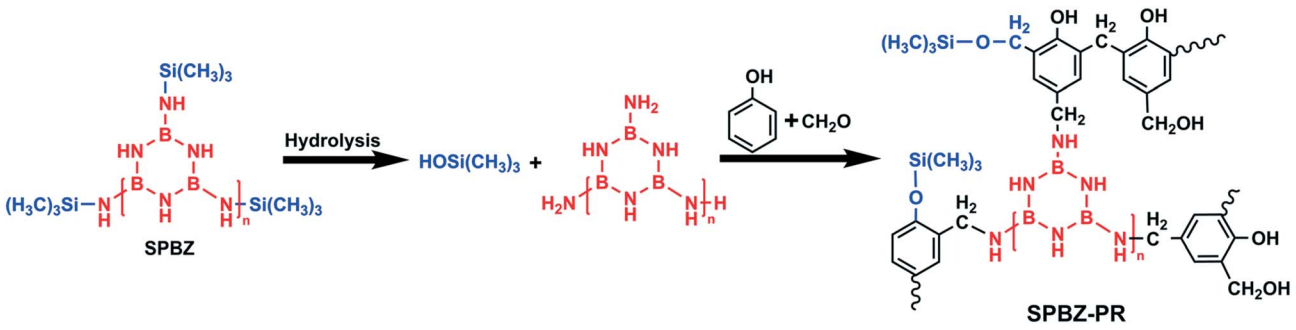

Scheme 1 Schematic diagram of synthesizing SPBZ-PR.

(TGA), thermogravimetry-mass spectrum analysis (TG-MS), X-ray photoelectron spectroscopy (XPS), Fourier transform infrared (FTIR) and Raman analyses were performed to characterize and investigate the chemical structures, thermal stabilities, and structural evolution during pyrolysis process of the SPBZ-PR. In addition, the corresponding ablation resistance and mechanical properties of the CF/PR and CF/SPBZ-PR composites were also investigated.

2. Experimental

2.1. Main materials

Phenol, paraformaldehyde, alkaline catalyst and *n*-hexane were all purchased from Tianjin Chemical Reagent Co., Tianjin, China. Borontrichloride and hexamethyldisilazane were both received from Beijing Huawei-Ruike (HWRK) Chem. Co., Ltd., Beijing, China. Carbon fibers (GQ3522 1K) were purchased from Weihai Guangwei Composites Co., Ltd.

2.2. Synthesis of SPBZ-PR

Molten phenol (0.5 mol) was added into 250 mL three-necked flask. And the SPBZ, alkaline catalyst (4wt% of phenol) and paraformaldehyde (1.3 molar ratio of phenol) were then added into the above three-necked flask in sequence. The obtained mixtures were maintained at 80°C until the solution became transparent. Finally, the above products were kept in the vacuum oven at -0.095 MPa, finally to obtain the yellow semi-solid transparent resins (SPBZ-PR). The corresponding schematic diagram of synthesizing SPBZ-PR was presented in Scheme 1. The SPBZ-PR with 5, 8.8, 10, 15, 20 wt% of phenol to SPBZ was named as $SPBZ_5$-PR, $SPBZ_{8.8}$-PR, $SPBZ_{10}$-PR, $SPBZ_{15}$-PR and $SPBZ_{20}$-PR, respectively. And the SPBZ-PR was cured according to the procedure of 110°C/1h+160°C/2h, followed by post-curing at 220°C for another 4h. And the pyrolysis process of cured SPBZ-PR was heated to the targeted temperature (400°C, 600°C, 800°C, 1000°C and 1200°C) under argon atmosphere from ambient temperature at 5°C/min and kept for 2 h.

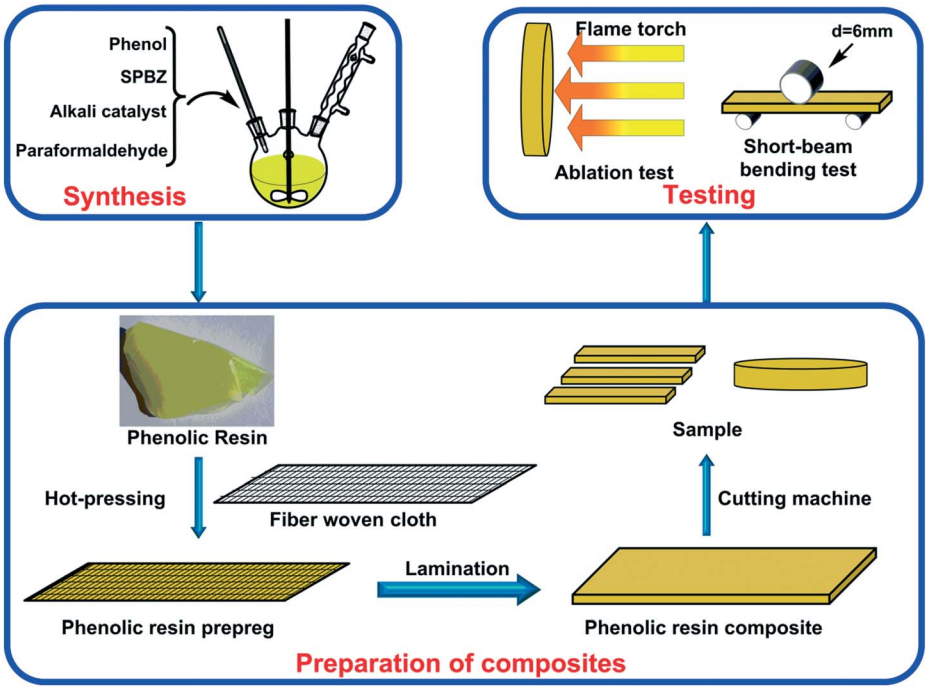

Fig. 1 Schematic diagram of the fabrication for the CF/SPBZ-PR composites.

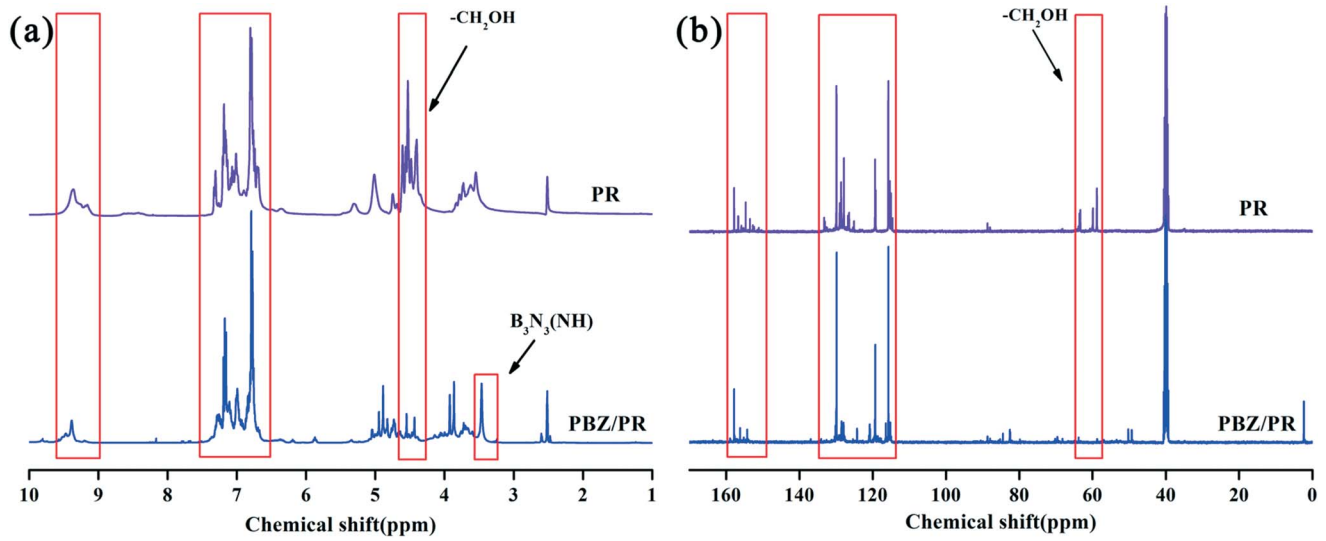

Fig. 2 NMR spectra of PR and $SPBZ_{15}$-PR. (a) ^{1}H NMR, (b) ^{13}C NMR.

2.3. Preparation of CF/SPBZ-PR laminated composites

Carbon fibers (CF) woven cloth was firstly tailored into square (120 mm ×120 mm). The corresponding CF/SPBZ-PR prepregs were prepared by hot melt method, which were then laminated and hot pressed at 5 MPa according to the procedure of 110 °C/1 h+160 °C/2 h, followed by post-curing at 220 °C for another 4 h. The schematic diagram of the fabrication for the CF/SPBZ-PR laminated composites was presented in Figure 1.

3. Results and discussion

3.1. Structure characterization of SPBZ-PR

Characteristic signal at 28.1 ppm in Figure S2 can be assigned to borazine ring.[39] From Scheme 1, Si-N bond of SPBZ can be hydrolyzed to generate primary amine and silanol. And then borazine ring can be successfully incorporated into PR matrix *via* condensation polymerization between phenol, paraformaldehyde and primary amine. And the NMR spectra of PR and $SPBZ_{15}$-PR are presented in Figure 2. The signals at 4.2-4.6 ppm in ^{1}H NMR and 58.0-64.0 ppm in ^{13}C NMR can be assigned to hydroxymethyl group,[1] and the intensities of $SPBZ_{15}$-PR are evidently weakened compared with that of PR. The characteristic peak at 3.4 ppm in ^{1}H NMR is ascribed to borazine ring,[40] also proven by absorption peak at 1457 cm^{-1} in FTIR (Figure S3). In addition, the absorption peak of C-N is observed at 1645 cm^{-1}. Peak at 989 cm^{-1} and 1076 cm^{-1} can be attributed to the Si-O-Ph and Si-O-CH_2 structure, respectively.[41,42] Si-O-C structures are formed by the reaction between silanol and phenolic hydroxyl group or hydroxymethyl. The weak absorption peak at 1100 cm^{-1} can be assigned to the Si-O-Si structure.[43]

3.2. Thermal stabilities of the cured SPBZ-PR

TGA and DTG curves of the cured PR and SPBZ-PR are shown in Figure 3, and the characteristic thermal data are also presented in Table S1. The decomposition temperatures (T_5, T_{10} *and* T_{max})[44,45] and

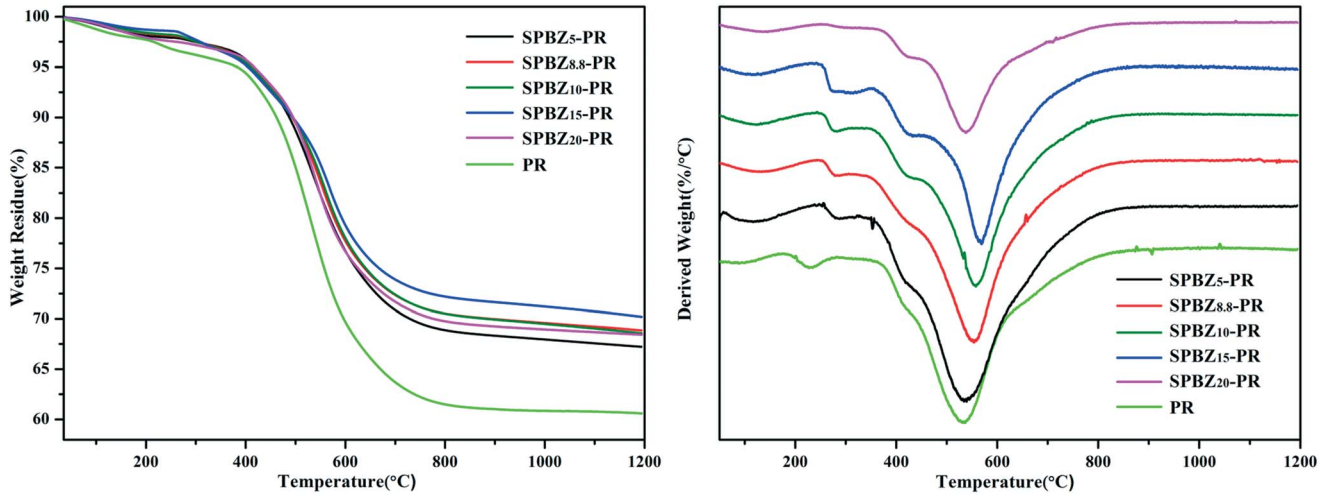

Fig. 3 TGA and DTG curves of the cured PR and SPBZ-PR. (a) TGA, (b) DTG.

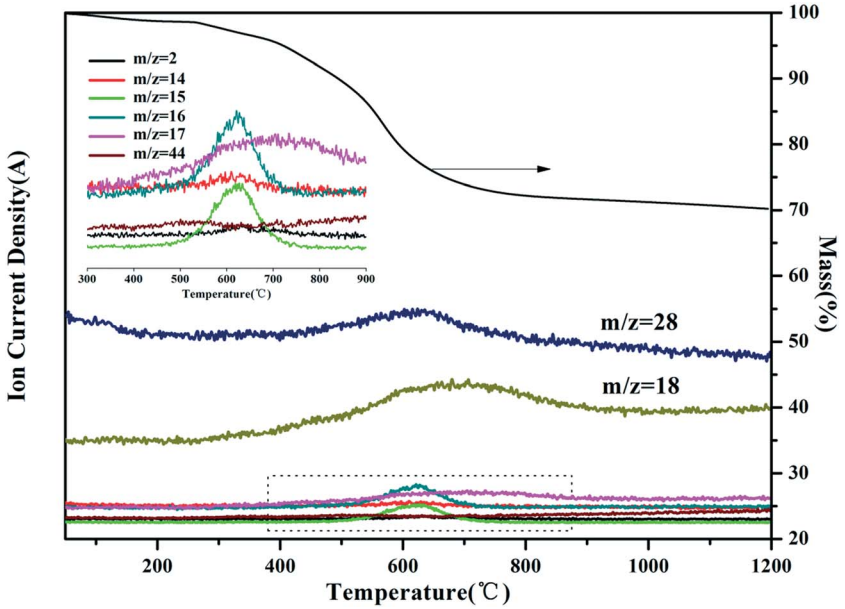

Fig. 4 TGA-mass curves of the cured $SPBZ_{15}$-PR.

char yield of the SPBZ-PR are all higher than that of PR. When the content of SPBZ is lower than 15%, the C_{800} and T_{max} of the SPBZ-PR are both increased with the increasing addition of SPBZ. For $SPBZ_{20}$-PR, the C_{800} is lower than that of $SPBZ_{15}$-PR, which might be ascribed to the incomplete polymerization.[38] It can be also seen that the $SPBZ_{15}$-PR presents the optimal thermal stability, the corresponding T_5, T_{10} *and* T_{max} is enhanced to 406.8°C, 496.6°C and 570.4°C, respectively, all higher than that of the PR. C_{800} and C_{1000} of $SPBZ_{15}$-PR is 72.5% and 71.2%, respectively, also higher than that of PR (C_{800} of 61.4% and C_{1000} of 60.8%). Particularly, C_{1200} of the $SPBZ_{15}$-PR still retains 70.3%. It demonstrates that the introduction of SPBZ can not only improve the thermal decomposition temperatures of PR, but also increase the char yield at higher temperatures (>800°C).

3.3. Structure evolution of the $SPBZ_{15}$-PR during pyrolysis process

The pyrolysis mechanisms (schizolytic molecule evolution and structure change) of the cured $SPBZ_{15}$-PR during pyrolysis are investigated by TG-MS, XPS and FTIR. The schizolytic molecule evolution of the cured $SPBZ_{15}$-PR during pyrolysis can be analyzed by TG-MS (Figure 4). The thermolysis of the cured $SPBZ_{15}$-PR can be mainly accompanied by the evolution of H_2 (m/z = 2), hydrocarbons such as CH_x^+ (x = 1-3, m/z = 13-15) and CH_4 (m/z = 16), OH^+ (m/z = 17), H_2O (m/z = 18), CO (m/z = 28), as well as CO_2 (m/z = 44). From 400°C to 800°C, the formation of CH_4 and its cation fragments CH_x^+ can be linked to the rearrangement and decomposition of Si-CH_3 groups and methylene bridged (-CH_2-). H_2 is generated by dehydrocoupling and carbonization of carbon networks at 500-800°C. The evolution of H_2O and its fraction OH^+ mainly occur at 300-1000°C, caused by the condensation and elimination of phenolic hydroxyl groups and the oxidation of terminal groups (CH_4 and H_2). It can be deduced that the CH_4 and H_2 can be released over 400°C, and the corresponding weight loss can be mainly ascribed to the condensation reaction of phenolic hydroxyl. The release of CO at 400-900°C and CO_2 at 400-800°C can be derived from the destruction of carbonyl and carboxyl groups formed by the scission and oxidation of methylene.

The structure evolution of the cured $SPBZ_{15}$-PR during pyrolysis can be investigated using FTIR in Figure 5. Peak intensity of aliphatic C-H at 2800-3000 cm^{-1} and -Si(CH_3)$_3$ at 1250 cm^{-1} is reduced from 400°C to 800°C. Simultaneously, the stretching vibration absorption peak of the C-H on the benzene ring at 3000-3100 cm^{-1} is also gradually weakened. Peak at 1602 cm^{-1} can be assigned to the stretching vibration of the C=C on aromatic ring, resulted from the volatilization of phenol and its derivatives, indicating the preliminary formation of char networks.[46,47] The intensity of absorption peak for Si-O-Si structure is

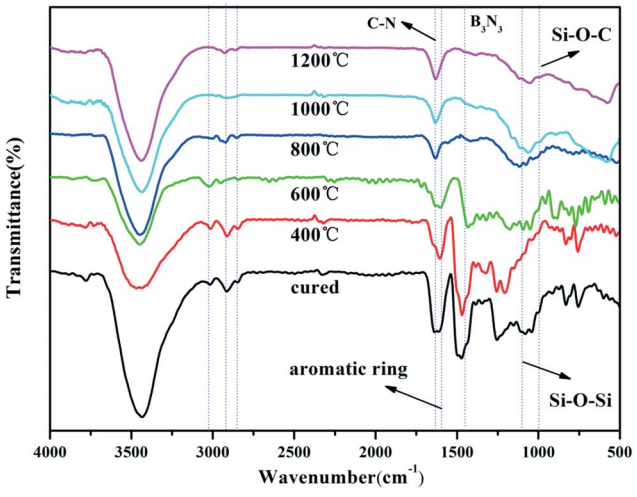

Fig. 5 FTIR spectra of the cured $SPBZ_{15}$-PR.

gradually increased with the increasing temperature. However, the peak at 990 cm^{-1} for Si-O-C structure is reduced. The existence of SiOx structure makes a major contribution to higher char yield of $SPBZ_{15}$-PR. Furthermore, the B_3N_3 structure at 1450 cm^{-1} from 220°C to 1200°C reveals that the SPBZ in pyrolysis products is beneficial to improving the char yield.

Figure 6 shows the C1s XPS spectra of the cured $SPBZ_{15}$-PR treated at different temperatures. There is no difference of the chemical bonding for cured $SPBZ_{15}$-PR treated at 400°C. The existence of C-N bond can prove the $SPBZ_{15}$-PR has been obtained. In addition, noncovalent π-π* stacking of aromatic ring with C1s binding energy of 291.3 eV can be detected. The chemical state C=O is also

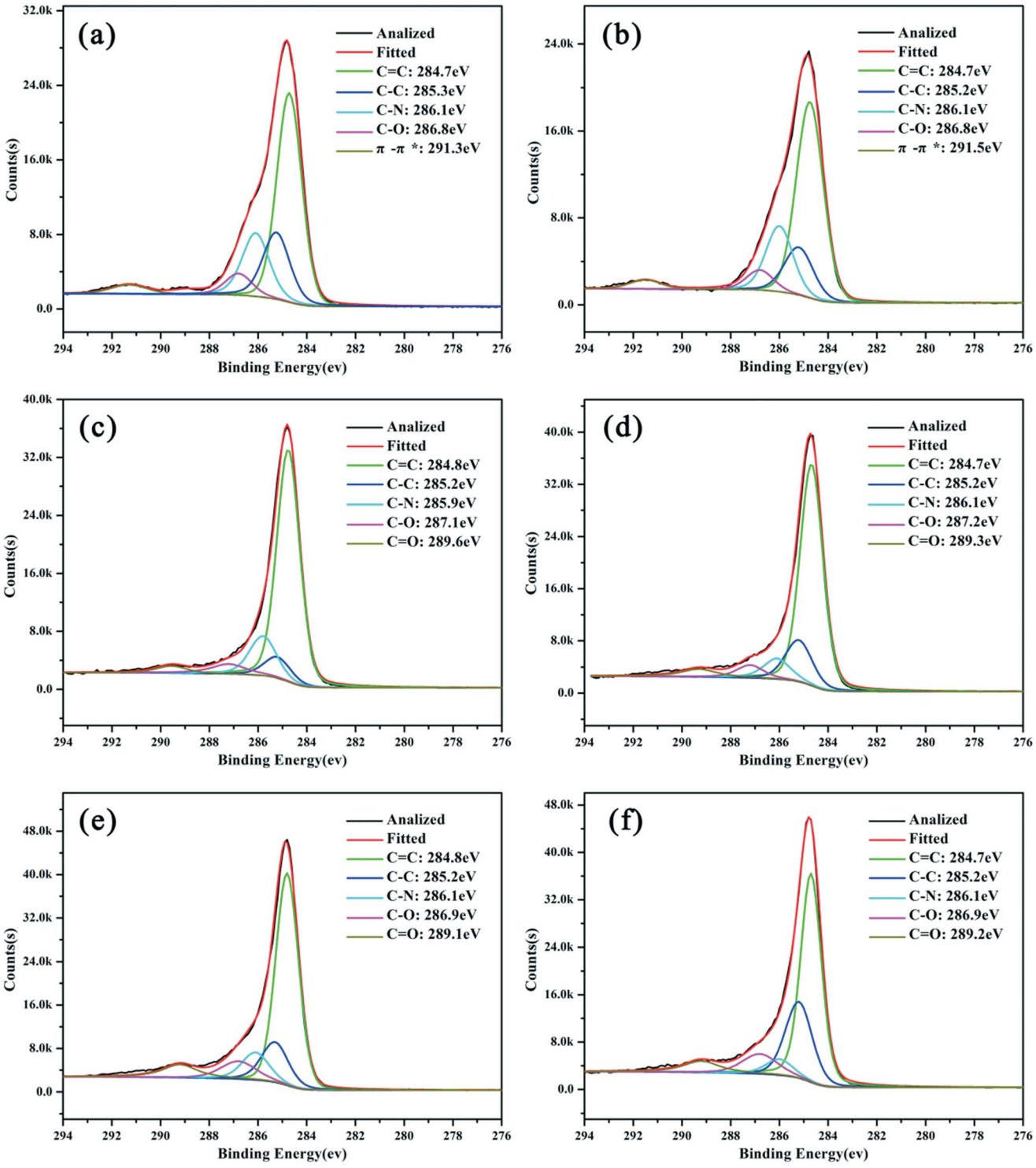

Fig. 6 C1s XPS spectra for cured $SPBZ_{15}$-PR treated at different temperatures. (a) cured $SPBZ_{15}$-PR, (b) 400°C, (c) 600°C, (d) 800°C, (e) 1000°C, (f) 1200°C.

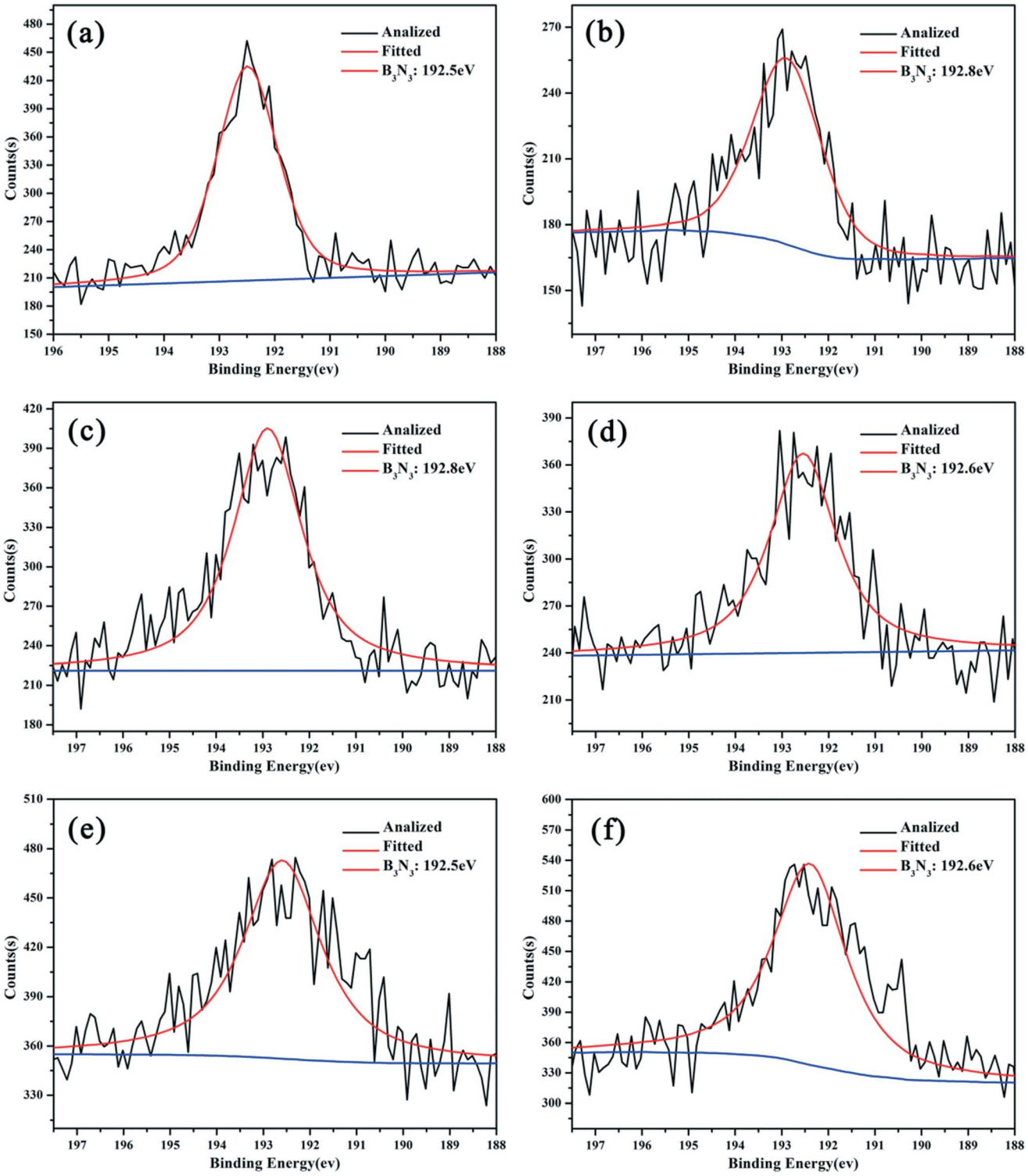

Fig. 7 B1s XPS spectra for cured $SPBZ_{15}$-PR treated at different temperatures. (a) cured $SPBZ_{15}$-PR, (b) 400°C, (c) 600°C, (d) 800°C, (e) 1000°C, (f) 1200°C.

appeared at 600°C (Figure 6c) and is gradually increased from 600°C to 1200°C, mainly ascribed to the oxidation of methylene groups.[48–50] The corresponding B1s high-resolution XPS spectra of the cured $SPBZ_{15}$-PR treated at different temperatures are also shown in Figure 7. The single characteristic peak at 192.4 eV indicates that B atom in cured $SPBZ_{15}$-PR treated at different temperatures presents only one chemical environment, assigned to the six-membered borazine ring.[51,52] It further demonstrates that the introduction of six-membered borazine ring can enhance the thermal stability of the $SPBZ_{15}$-PR. Si2p XPS spectra for the cured $SPBZ_{15}$-PR treated at different temperatures are also presented in Figure 8. Si-O-C and Si-Ox bond with Si2p at 102.2 eV and 103.5 eV can be detected

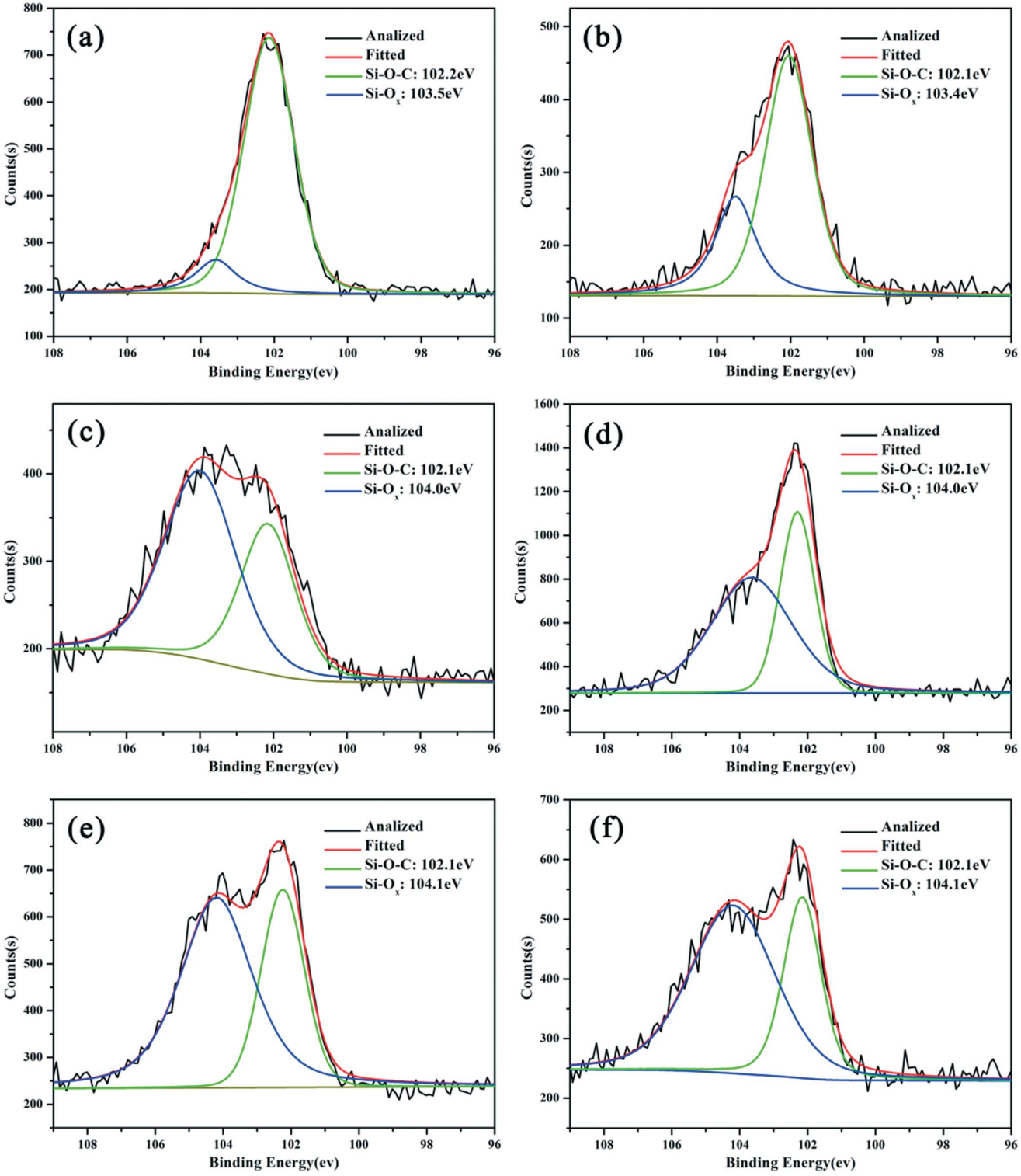

Fig. 8 Si2p XPS spectra for cured $SPBZ_{15}$-PR treated at different temperatures. (a) cured $SPBZ_{15}$-PR, (b) 400°C, (c) 600°C, (d)800°C, (e) 1000°C, (f) 1200°C.

and the proportion of Si-O-C and Si-O_x is also shown in Table S2. The content of the Si-O-C is reduced and its proportion at 1200°C is 32.24%. For Si-O_x structure, its proportion is increased from 11.78% to 67.76% at 1200°C. One hand, the Si-O-C of the cured $SPBZ_{15}$-PR can be hydrolyzed to generate Si-OH and C-OH over 400°C,[53] and the condensation reaction between Si-OH can occur to obtain Si-Ox. On the other hand, phenolic hydroxyl groups are good for generating hydroxyl radicals, and the Si-CH_3 can be converted into the Si-OH and methyl radical under the hydroxyl radicals above 500°C,[54] finally to form the Si-O_x.

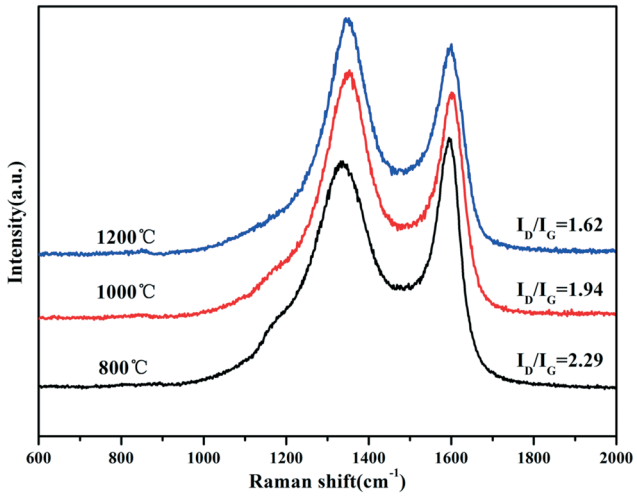

Fig. 9 Raman spectra of $SPBZ_{15}$-PR.

Figure 9 presents the Raman spectra of the cured $SPBZ_{15}$-PR treated at different temperatures. D-band at 1350 cm^{-1} corresponds to defect lattice vibration mode associated with disordered carbon structure,[55] and G-band caused by the in-plane bond stretching of sp2 carbons near 1600 cm^{-1} represents the graphite structure. The I_D/I_G intensity ratio stands for the degree of crystallinity by the Gaussian-Lorentzian fitting. The I_D/I_G value of the treated $SPBZ_{15}$-PR is decreased from 2.29 to 1.62 from 800°C to 1200°C, lower than that of PR at the same treated temperatures. It can be deduced that the introduction of $SPBZ_{15}$ into PR matrix can decrease the disordered structure and form graphite structure.

Based on the above analyses, the structure evolution of $SPBZ_{15}$-PR may be caused by following three reasons: (i) Borazine rings can steadily exist during the whole pyrolysis process; (ii) Si-O_x structure can be formed with the increasing temperature; (iii) The introduction of $SPBZ_{15}$ can promote the degree of graphitization of pyrolysis products.

Table 1 ILSS values, linear and mass ablation rate of the CF/PR and CF/$SPBZ_{15}$-PR.

Composites	ILSS values (MPa)			Resin content (%)	Linear ablation rate (mm/s)	Mass ablation rate (g/s)
	Untreated	500°C	800°C			
CF/PR	15.5	2.3	1.9	34.8%	0.013	0.033
CF/$SPBZ_{15}$-PR	36.0	8.8	2.9	32.1%	0.0079	0.025

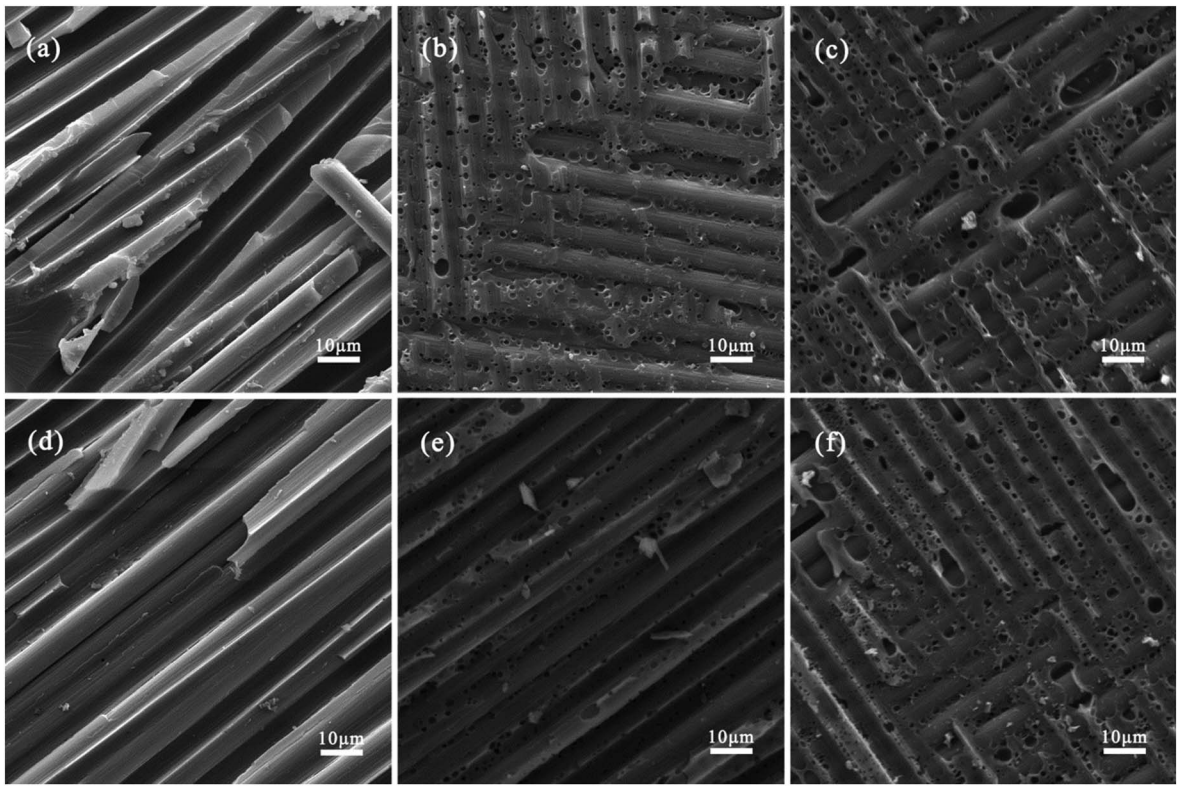

Fig. 10 Morphologies of interfaces of the composites. (a) CF/PR, (b) CF/PR treated at 500°C, (c) CF/PR treated at 800°C, (d) CF/$SPBZ_{15}$-PR, (e) CF/$SPBZ_{15}$-PR treated at 500°C, (f) CF/$SPBZ_{15}$-PR treated at 800°C.

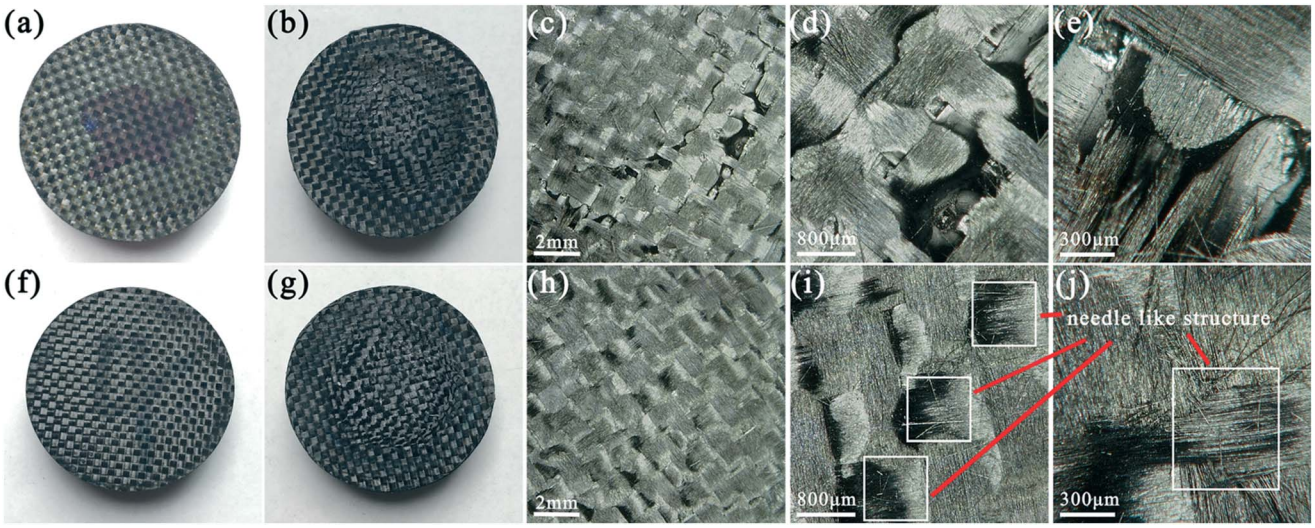

Fig. 11 Images of the composites before and after ablation. (a) photograph of CF/PR before ablation, (b) photograph of CF/PR after ablation, (c)-(e) digital microscope images of CF/PR after ablation; (f) photograph of CF/SPBZ$_{15}$-PR before ablation, (g) the photograph of CF/SPBZ$_{15}$-PR after ablation, (h)-(j) digital microscope images of CF/SPBZ$_{15}$-PR after ablation.

3.4. ILSS and ablation properties of the CF/SPBZ$_{15}$-PR laminated composites

Table 1 shows the ILSS values, linear & mass ablation rate of the CF/PR and CF/SPBZ$_{15}$-PR laminated composites. The ILSS value (36.0 MPa) of the CF/SPBZ$_{15}$-PR laminated composites is higher than that of CF/PR (15.5 MPa), mainly ascribed to relatively stronger interfacial interaction between CF and SPBZ$_{15}$-PR matrix. And the PR and SPBZ$_{15}$-PR are both dense and CF is arranged in parallel. In addition, there is no obvious debonding at the interfaces (Figure 10a, d), indicating good interfacial compatibility. The corresponding ILSS values of the CF/PR and CF/SPBZ$_{15}$-PR laminated composites are decreased significantly after heat treatment and dwindled with the increasing temperature. After the heat treatment at 500^{o}C, the ILSS value of the CF/PR and CF/SPBZ$_{15}$-PR laminated composites is decreased to 2.3 MPa and 8.8 MPa, respectively. And after the heat treatment at 800^{o}C, the ILSS value of the CF/PR and CF/SPBZ$_{15}$-PR laminated composites is further decreased to 1.9 MPa and 2.9 MPa, respectively. It is mainly ascribed to the formation of holes and cracks at the interfaces during pyrolysis process (Figure 10b, d-f).

The linear and mass ablation rate are both decreased from 0.013 mm/s and 0.033 g/s for CF/PR laminated composites to 0.0079 mm/s and 0.025 g/s for CF/SPBZ$_{15}$-PR laminated composites, decreased by 39.2% and 24.2%, respectively. It reveals that the CF/SPBZ$_{15}$-PR laminated composites presents more excellent ablation performance. Form Figure 11, the surfaces of the CF/PR and CF/SPBZ$_{15}$-PR laminated composites after ablation are sunken (Figure 11b, g). And there are slight cracks on the partial surface of CF/PR laminated composites (Figure 11c, d), while the surface of the CF/SPBZ$_{15}$-PR laminated composites is more intact (Figure 11h, i). It reveals that the CF/SPBZ$_{15}$-PR laminated composites presents more excellent shape retention ability after ablation. In addition, the CF in CF/PR laminated composites also suffers severe destruction (Figure 11d, e), while the CF in CF/SPBZ-PR laminated composites presents less breakage by needle-like structure formation (Figure 11i, j), due to higher decomposition temperature and char yield.[56] All evidences indicate that the ablation performance of CF/SPBZ$_{15}$-PR laminated composites is superior to that of CF/PR laminated composites.

4. Conclusion

SPBZ-PR had been fabricated successfully *via* condensation polymerization between phenol, paraformaldehyde and primary amine. The incorporation of SPBZ could obviously improve the thermal stabilities of PR matrix, and the corresponding optimal T_5 of the SPBZ-PR$_{15}$ was increased to 406.8^{o}C and the char yield at 1200^{o}C still retained 70.3%. The improvement of char yield for SPBZ$_{15}$-PR might be caused by following reasons: (i) Borazine rings could steadily exist during the whole pyrolysis process; (ii)Si-O$_x$ structure could be formed with the increasing temperature; (iii) The introduction of SPBZ$_{15}$ could promote the degree of graphitization of pyrolysis product for PR. The CF/SPBZ$_{15}$-PR laminated composites presented relatively higher ILSS value and lower linear & mass ablation rate than that of CF/PR laminated composites. Especially, the linear ablation rate and mass ablation rate were both decreased from 0.013 mm/s and 0.033 g/s for CF/PR laminated composites to 0.0079 mm/s and 0.025 g/s for CF/SPBZ$_{15}$-PR laminated composites, decreased by 39.2% and 24.2%, respectively. Moreover, CF/SPBZ$_{15}$-PR laminated composites also presented more excellent shape retention ability after ablation.

Acknowledgements

The authors are grateful for Shenzhen Science and Technology Innovation Fund (No. JCYJ20170815155705061); Space Supporting Fund from CASIC (No. 2017-HT-XG); Shanghai Aerospace Science and Technology Innovation Fund (No. SAST2017-121); Fundamental Research Funds for the Central Universities (No. 3102017jg02003);

and the Seed Foundation of Innovation and Creation for Graduate Students in Northwestern Polytechnical University (No. Z2017046). We would like to thank the Analytical & Testing Center of Northwestern Polytechnical University for test and characterization.

References

1 M. O. Abdalla, A. Ludwick and T. Mitchell, *Polymer*, 2003, **44**, 7353–7359.
2 Q. Li, L. Chen, X. Li, J. Zhang, X. Zhang, K. Zheng, F. Fang, H. Zhou and X. Tian, *Compos. Part A-Appl. S*, 2016, **82**, 214–225.
3 Y. Xu, J. Zhu, Z. Wu, Y. Cao, Y. Zhao and W. Zhang, *Adv. Compos. Hybrid Mater.*, 2018, 1–18.
4 A. R. Bahramian, M. Kokabi, M. H. Navid Famili and M. H. Beheshty, *Polymer*, 2006, **47**, 3661–3673.
5 W. Haikun, Y. Zhang, R. Yin, W. Zhao, X. Li and L. Qian, *Adv. Compos. Hybrid Mater.*, 2018, **1**, 168–176.
6 X. Yang, Y. Guo, X. Luo, N. Zheng, T. Ma, J. Tan, C. Li, Q. Zhang and J. Gu, *Compos. Sci. Technol.*, 2018, **164**, 59–64.
7 M. Tripathi, D. Kumar and P.K. Roy, *Compos. Commun.*, 2018, **4**, 20–23.
8 X. Yang, C. Liang, T. Ma, Y. Guo, J. Kong, J. Gu, M. Chen and J. Zhu, *Adv. Comp. Hybrid Mater.*, 2018, **1**, 207–230.
9 F. Fang, G. Huang, H. Xiao, Y. Li, N. Hu and S. Fu, *Compos. Sci. Technol.*, 2018, **156**, 144–150.
10 J. Gu, Z. Lv, Y. Wu, Y. Guo, L. Tian, H. Qiu, W. Li and Q. Zhang, *Compos. Part A-Appl. S*, 2017, **94**, 209–216.
11 Y. Tang, W. Dong, L. Tang, Y. Zhang, J. Kong and J. Gu, *Compos. Commun.*, 2018, **8**, 36–41.
12 L. Wan, X. Zhang, G. Wu and A. Feng, *The Int. Eng. Technol.*, 2017, **2**, 167–171.
13 G. L. Vignoles, Y. Aspa and M. Quintard, *Compos. Sci. Technol.*, 2010, **70**, 1303–1311.
14 M. H. Choi, B. H. Jeon and I. Chung, *Polymer*, 2000, **41**, 3243–3252.
15 J. Feng, J. Li, L. Chen, Y. Qin, X. Zhang, J. Gu, S. Tadakamallac and Z. Guo, *J. Polym. Res.*, 2017, **24**, 176–187.
16 J. Wang, H. Jiang and N. Jiang, *Thermochim. Acta*, 2009, **496**, 136–142.
17 G. Cameron and E. James, *Carbon*, 1995, **33**, 389–395.
18 X. Yang, L. Tang, Y. Guo, C. Liang, Q. Zhang and K. Kou, et al., *Compos. Part A-Appl. S*, 2017, **101**, 237–242.
19 C. Feng, L. Bai, R. Bao, Z. Liu, M. Yang, J. Chen and W. Yang, *Adv. Compos. Hybrid Mater.*, 2018, **1**, 160–167.
20 K. Haraguchi, Y. Usami, K. Yamamura and S. Matsumoto, *Polymer*, 1998, **39**, 6243–6250.
21 J. Gu, Q. Zhang, H. Li, Y. Tang, J. Kong and J. Dang, *Polymer-Plastics Technol. Eng.*, 2007, **46**, 1129–1134.
22 A. Saghar, K. Khan, I. Sadiq and T. Subhani, *Vacuum*, 2018, **148**, 124–126.
23 S. H. Yum, S. H. Kim, W. I. Lee and H. S. Kim, *Compos. Sci. Technol.*, 2015, **121**, 16–24.
24 Y. Tang, J. Kong, J. Gu and G. Liang, *Polymer-Plastics Technol. Eng.*, 2009, **48**, 359–366.
25 X. Shen, Z. Wang, Y. Wu, X. Liu, Y. He and J. Kim, *Nano Lett.*, 2016, **16**, 3585–3593.
26 Z. Zhang, M. Song, J. Hao, K. Wu, C. Li and C. Hu, *Carbon*, 2018, **127**, 287–296.
27 L. Chen, X. Hou, N. Song, L. Shi and P. Ding, *Compos. Part A-Appl. S*, 2018, **107**, 189–196.
28 Y. Guo, G. Xu, X. Yang, K. Ruan, T. Ma, Q. Zhang, J. Gu, Y. Wu, H. Liu and Z. Guo, *J. Mater. Chem. C*, 2018, **6**, 3004–3015.
29 J. Gao, C. Jiang and X. Su, *Int. J. Polym. Mater.*, 2010, **59**, 544–552.
30 Y. Zhang, S. Lee, M. Yoonessi, K. Liang and C. Pittman, *Polymer*, 2006, **47**, 2984–2996.
31 M. A. Espinosa, M. Galià and V. Càdiz, *J. Polym. Sci. A Poly. Chem.*, 2004, **42**, 3516–3526.
32 H. Shen, J. Zheng and X. Huang, *Compos. Struct.*, 2003, **60**, 57–66.
33 C. Martín, J. Ronda and V. Cádiz, *J. Polym. Sci. A Poly. Chem.*, 2006, **44**, 3503–3512.
34 A. M. Kawamoto, L. C. Pardini, M. F. Diniz, V. L. Lourenço and M. Takahashi, *J. Aerosp. Technol. Manag.*, 2010, **2**, 169–182.
35 J. Yun, L. Chen, X. Zhang, J. Feng and L. Lin, *Ploymers*, 2016, **8**, 35–42.
36 J. Kong, M. Wang, J. Zou and L. An, *ACS Appl. Mater. Interf.*, 2015, **7**, 6733–6744.
37 H. Zhao, J. Zhao, H. Li and T. Zhao, *Chinese J. Polym. Sci.*, 2014, **32**, 187–196.
38 Y. Wang, L. Chen, T. Xu, Y. Yan, J. Gu and J. Yun, et al., *Polym. Degrad. Stabil.*, 2017, **137**, 184–196.
39 H. Nöth and B. Wrackmeyer, *Springer Sci. Bus. Media*, 2012, **14**, 154–167.
40 P. Miele, B. Toury, D. Cornu and S. Bernard, *J. Organomet. Chem.*, 2005, **36**, 2809–2814.
41 K. Drake, I. Mukherjee, K. Mirza, F. Ji, J. Bradley and Y. Wei, *Macromolecules*, 2013, **46**, 4370–4377.
42 J. Yun, L. Chen, X. Zhang, H. Zhao, Z. Wen and C. Zhang, *Polym. Degrad. Stabil.*, 2017, **139**, 97–106.
43 C. Li, Z. Ma, X. Zhang, H. Fan and J. Wan, *Thermochim. Acta*, 2016, **639**, 53–65.
44 J. Gu, W. Dong, S. Xu, Y. Tang, L. Ye and J. Kong, *Compos. Sci. Technol.*, 2017, **144**, 185–192.
45 Y. Li, G. Xu, Y. Guo, T. Ma, X. Zhong, Q. Zhang and J. Gu, *Composites Part A*, 2018, **107**, 570–578.
46 Y. Zhao, N. Yan and M. Feng, *Thermochim. Acta*, 2013, **555**, 46–52.
47 M. S. Chetan, R. S. Ghadage, C. R. Rajan, V. G. Gunjikar and S. Ponrathnam, *J. Appl. Polym. Sci.*, 1993, **50**, 685–692.
48 W. M. Jackson and R. T. Conley, *J. Appl. Polym. Sci.*, 1964, **8**, 2163–2193.
49 E. Fitzer and W. Schäfer, *Carbon*, 1970, **8**, 353–364.
50 S. Wang, Y. Wang, C. Bian, Y. Zhong and X. Jing, *Appl. Surf. Sci.*, 2015, **331**, 519–529.
51 M. Jansen, B. Jäschke and T. Jäschke, *Germany: Springer Berlin Heidelberg Stuttgart*, 2002, **101**, 137–191.
52 S. Dong, W. Han, Y. Luo, T. Zhao and C. Xu, *J. Mater. Sci. Technol.*, 2010, **26**, 228–233.
53 B. Kumar and Y. Kim, *Sci. Technol. Adv. Mat.*, 2010, **11**, 69801–69803.
54 S. C. Zunjarrao, A. Rahman and R. P. Singh, *J. Am. Ceram. Soc.*, 2013, **96**, 1869–1876.
55 M. J. Matthews, M. A. Piment, G. Dresselhaus, M. S. Dresselhaus and M. Endo, *Phys. Rev. B*, 1999, **59**, 6585–6588.
56 D. Cho and B. I. Yoon, *Compos. Sci. Technol.*, 2001, **61**, 271–280.

